Supplementary Mask Fabrication Methods

For 3D printed respirator designs, a number of different 3D printers and materials were used depending on availability. For sewn respirators, traditional sewing machines were used by experienced sewers. In all cases, fabrication followed the process defined in the online instructions. Detailed fabrication procedures for the five designs, named as follows in the main text: P100 Adaptor**,** Multi-part 3D Printed Mask, Sewn Sterilization Wrap, Commercial Elastomeric Respirator, Self-Moldable 3D Print. All links were retrieved on May 1, 2020.

Sewn Sterilization Wrap

The Florida mask pattern and instructions were downloaded from the University of Florida Department of Anesthesiology website.[1] Two layers of Halyard 600 sterilization wrap (Halyard, Alpharetta, GA) was cut according to the pattern downloaded and printed from the website. The masks were assembled with a Janome Memory Craft (Janome, Tokyo, Japan) home sewing machine according to the detailed instructions provided. Spandex elastic 3/8 inch (0.952 cm) wide was attached at the specified locations.

P100 Adaptor

Manufacture of the "P100 Adaptor" mask followed open source instructions created at the Barrow Innovation Center (Phoenix, AZ).[2] Mask parts were produced by fused deposition modeling 3D printing and silicone casting for fit. Parts were printed in PLA (grey stock 1.75 mm from Prusa) with 20% infill and a shell thickness of 4 perimeters using a .4 mm nozzle on a Prusa i3 MK3s. The print layer height was .2 mm thickness. Print temperature was 200°C with a print bed temperature of 70°C. A soldering iron was used to melt perforations in 3D printed mask perimeter. A mold was created from a production staff member's face, encasing the printed

Ballard DH, *et al. BMJ Open* 2022; 11:e045557. doi: 10.1136/bmjopen-2020-045557

shell of the mask with clay. This clay mold was then removed, and a silicone seal was cast. Assembly of the mask required manually clearing the holes in the plastic shell and trimming clearance for elastic head straps to pass silicone seal. An O-ring seal was applied prior to attachment of a p100 filter.

Specifications were followed as described in the document from the Barrow Innovation Center, with a few exceptions as follows. The silicone mold as described was observed to be too thick to obtain a completed seal, so the edge of mold was sculpted back for a better fit. Moreover, the seal as described did not stay adhered to the mask shell on first casting and had to be glued after removal from mold. Although the end user would ideally be present for mask production to ensure personalized fit, this was not possible in our fabrication process, and masks were molded to the face of a production staff member.

Self-Moldable 3D Print

"Self-Moldable 3D Print" masks designs were obtained from open source instructions provided by Make the Masks.[3] 3D printer files were formatted in Simplify3D (Simplify3D, Cincinnati, OH) for use on the Fusion3 F410 (Fusion 3D, Greensboro, NC) single filament printer with a 0.4 mm diameter print head and standard 1.75 mm PLA. Head temperature was set at 240°C. Test prints priors were conducted at infills of 10%, 15%, 20% and 25% with aspect ratios of 90%, 95%, and 100%, corresponding to small, medium, and large face sizes. These test prints were sanded, cleaned, and test fit to gauge pliability under heat molding as outlined by the designers. Lower infills yielded more pliable masks but ran the risk of allowing perforations in the print layers that compromised the integrity of the mask. After these preliminary test prints, prototype

samples were printed with a print head temperature of 230°C, with extrusion and print speeds lowered to 90%, and monitored for the duration of the print to ensure quality of layer adhesion at an infill of 15% in aspect ratios of 90% and 100%. Masks were individually molded to user faces using a hot water dip and adequate molding was established by forcibly exhaling against a blocked filter to identify points of air leak prior to quantitative testing.

Multi-part 3D Printed Mask

Manufacture of the "Multi-part 3D Printed Mask" closely followed open source instruction provided online by River City Labs.[4] Parts were printed in PLA (grey stock 1.75 mm from Prusa, Prague, Czech Republic) with 20% infill and a shell thickness of 3 perimeters using a .4 mm nozzle on a Prusa i3 MK3s. The print layer height was .2 mm thickness. Print temperature was 200°C with a print bed temperature of 70°C. Notably, a deviation in the printing process from the instructions was use of PLA rather than Polyethylene Terephthalate Glycol-modified (PETG) due to supply availability. For filtration material, Merv 13 (AAF International, Doraville, GA) was substituted for Merv 16 due to local supply limitations. After 3-D printing from the file provided and testing the seal mold, adjustments to the external geometry were needed to enable fitting. To address this, an alternative seal mold external geometry was developed to allow for better closure, but this still failed to yield a perfect seal. Seals did not self-retain on the contoured mask shell due to low elasticity of the seals, requiring gluing to the shell edge. Additionally, extensive hand finishing was not performed on exterior parts or on threads of articulating parts due to increasing thread tolerance and worsening seal.

Commercial Elastomeric Respirator

Instruction for fabrication were obtained from open source documents provided on the Boston Children's Hospital Website.[5] The "Commercial Elastomeric Respirator" was fabricated by mounting a Ultipor 25 Ventilator Inline Bacterial/Viral Filter (Pall Corporation, Westborough, MA) on an anesthesia face mask with one end open to the environment. A face piece-filter adapter with integrated sampling port was 3D printed of polylactic acid (PLA) using fused deposition modeling (Prusament PLA; Prusa i3 MK3S, Prusa Research, Prague, CZ). The sampling port was tapped to receive a 1/4 inch-28 compression fitting to seal around fluorinated ethylene propylene (FEP) tubing with an outer diameter of 1/8 in (3.12 mm). The mask was then secured using elastic straps attached to the 4-pronged ring surrounding the inflow and outflow tract.

Supplementary Splatter testing Methods

For splatter testing, a Nordson EFD ValveMate 8000 (Nordson Corporation, Westlake, OH) with a 741V pneumatic valve generated the liquid jet. Fabrics, either as a single or a double layer, were secured using a 1/16 inch (0.159 cm) rubber cuff over a polyethylene terephthalate (PET) 3D printed backing form with the standard-specified dimensions. A 0.25 inch (0.635 cm) centering hole, drilled into an acrylic sheet, was placed approximately 0.5 inches (1.27 cm) from the respirator surface, and the valve with an 18 gauge needle was placed at a distance of 12 inches (30.5 cm). After impingement, fabrics were visually inspected for liquid penetration.

Supplementary Filtration Methods

A flow diagram of the particle testing station is provided in Figure S1. Sample discs of 47 mm were extracted directly from the mask or the sourced material sheet and placed in a stainless steel in-line filter holder (Pall #2220, Pall Corporation, Westborough, MA), which exposed a circular area of 35 mm diameter during filtration testing. A polydisperse NaCl aerosol was produced from a 1.0 %wt. NaCl solution in DI water using a Collison Nebulizer (CH Technologies) and an in-line custom diffusion dryer, with a pressure of 8 psig (55.2 kPa) and a flow rate of 6 liters per minute (LPM). The aerosol was then passed through an electrostatic classifier (TSI Inc., Model 3080, Shoreview, MN, with long differential mobility analyzer (DMA) column, operated with a sheath flowrate of 5 LPM and an aerosol flow rate of 1.46 LPM ± 0.04, which was set by controlling the pressure at the exit of the DMA by continually adjusting the needle valve to vacuum) to select particles based on mobility in the electric field with a peak mobility size of 300 nm mean diameter. Electric mobility is proportional to the ratio of particle charge and aerodynamic diameter (equivalent to diameter for spherical particles), such that for a given diameter setpoint, a set of particles of increasing diameter and discrete charge (ie. +1, +2, etc.) will be selected by the DMA. Since the mode of the nebulizer size distribution is less than the 300 nm setpoint and since the aerosol is neutralized prior to the DMA, the singly charged particles (with 300 nm diameter mode) will predominate. After the classifier, the aerosol was neutralized a second time by flowing through a tube with two imbedded Po-210 strips (NRD Staticmaster 2U500, Grand Island, NY) and then diluted with HEPA-filtered house air. In the case of samples at 4.38±0.05 LPM (corresponding to 7.6±0.1 cm/s face velocity to the exposed filter area), an additional 2.92 LPM of using HEPA-filtered house air was added to achieve a final particle number concentration in the range of 3000 - 4000 particles per cubic centimeter. To determine the filtration efficiency, the concentrations of particles upstream and downstream of the filter were measured using a

continuous condensation particle counter (TSI Inc., Model 3022A). Upstream and downstream particle concentrations were measured in immediate succession to mitigate impact of drift in nebulizer output over time. The flow through the filter material was varied to achieve a range of face velocities. The pressure drop across the filter material was measured with a magnehelic differential pressure gauge (Dwyer, Michigan City, IN) and the temperature and relative humidity of the gas passed through the filter was measured with an industrial probe (Dwyer HHT Series). Relative humidity and temperature were not actively controlled and were within the range of 8 and 21 % relative humidity and 19.4 and 21.1°C for the results presented here.

Methods of calculation

Particle filtration efficiency for a single punch was calculated from the unfiltered and filtered particle concentrations ($C_{Unfiltered}$ and $C_{Filtered}$ respectively):

$$(Filtration\ Efficiency) = 1 - \frac{C_{Filtered}}{C_{Unfiltered}}.$$

$C_{Unfiltered}$ and $C_{Filtered}$ were calculated as the mean of replicate measurements through the bypass line and filter respectively for the same punch:

$$C = \frac{1}{J}\sum_{j=1}^{J} \bar{x}_j$$

where $\bar{x}_j$ is the j^{th} replicate measurement (of a total of J) for a given condition (filtered or unfiltered) and is calculated from the mean concentration (#/cc) recorded by the condensation particle counter (CPC) (for at least 30 s at 1 s time resolution):

$$\bar{x}_j = \frac{1}{n_{CPC}} \sum_{i=1}^{n_{CPC}} x_i$$

where x_i is the i^{th} raw concentration datum (of a total of n_{CPC} data) recorded by the CPC. $C_{Unfiltered}$ was also corrected for particle penentration (99.4% ± 2.4) through the empty filter holder relative to the bypass line:

$$C_{Unfiltered} = (99.4\%) \cdot \frac{1}{J} \sum_{j=1}^{J} \bar{x}_j$$

The uncertainty in filtration efficiency is the combined uncertainty of the two measurements as well as the uncertainty in the measurement of particle penetration through the empty filter holder:

$$S_{Efficiency} = (1 - Filtration\ Efficiency) \sqrt{\left(\frac{2.4\%}{99.4\%}\right)^2 + \left(\frac{S_{Unfiltered}}{C_{Unfiltered}}\right)^2 + \left(\frac{S_{Filtered}}{C_{Filtered}}\right)^2}.$$

The uncertainty of the unfiltered or filtered particle concentration ($S_{unfiltered}, S_{filtered}$) for a punch was calculated as the combined error from the maximum relative CPC variability (S_{CPC}) observed for that condition and punch and the variability between replicate measurements of the filtered or unfiltered particle concentrations (S_{Punch}):

$$S = \sqrt{{S_{CPC}}^2 + {S_{Punch}}^2}$$

$$S_{CPC} = max\left(\frac{s_{CPC,j}}{\bar{x}_j \sqrt{n_{CPC}}}\right) \times C$$

where n_{CPC} is the number of CPC measurements and $s_{CPC,j}$ is the standard deviation of the raw CPC data:

$$s_{CPC,j} = \sqrt{\frac{\sum_{i=1}^{n_{CPC}} \left(x_i - \bar{x}_j\right)^2}{n_{CPC} - 1}}$$

Given the evolving and urgent demand for this data, the number of replicates of measurements of $C_{Unfiltered}$ and $C_{Filtered}$ for a single punch ($n_{condition,unfiltered}$ and $n_{condition,filtered}$) varied from one unfiltered and one filtered measurement to three unfiltered and two filtered measurements (with the mean of each condition used to calculate filtration efficiency). These replicate measurements were always performed in immediate succession to mitigate any long-term nebulizer output drift. In cases where the unfiltered or filtered particle concentration $\bar{x}_j$ was measured multiple times for a single punch (with the mean value C used to calculate the particle capture efficiency), S_{Punch} was calculated as the standard error of the mean of these replicate measurements:

$$S_{Punch} = \frac{\sqrt{\frac{\sum\left(y_j - \bar{y}\right)^2}{n_{condition} - 1}}}{\sqrt{n_{condition}}}$$

where $n_{condition}$ is the number of replicate measurements for that condition and punch.

As discussed previously, for several punches, only a single unfiltered or filtered measurement were taken. Since a standard error cannot be computed for a single replicate, we estimated S_{Punch} using the standard error of an estimate calculated for the regression of repeat measurements (n=16 for unfiltered measurements, n=13 for filtered measurements) versus time in a separate test with the same sample flowrate and diameter setpoint. This approach yields estimates of $\frac{S_{Punch,filtered}}{C}$ of 1.43% and $\frac{S_{Punch,unfiltered}}{C}$ of 0.93%.

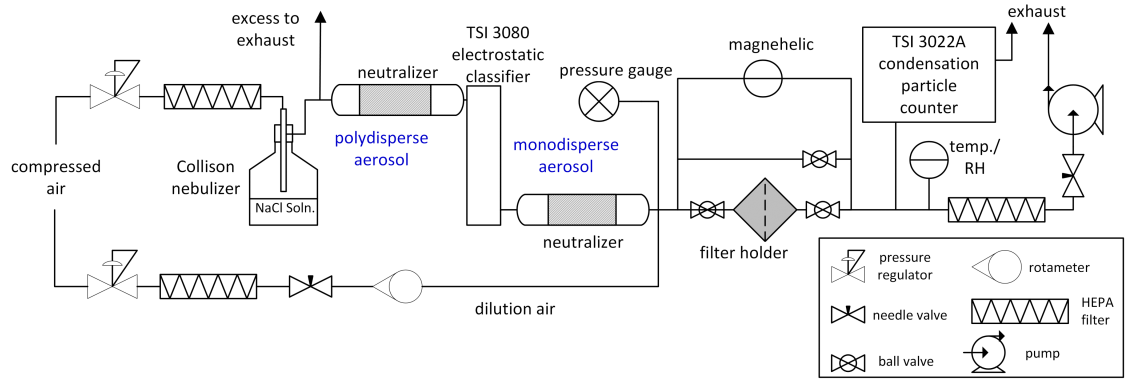

Supplemental Figure 1. Flow diagram of the aerosol filtration testing station.

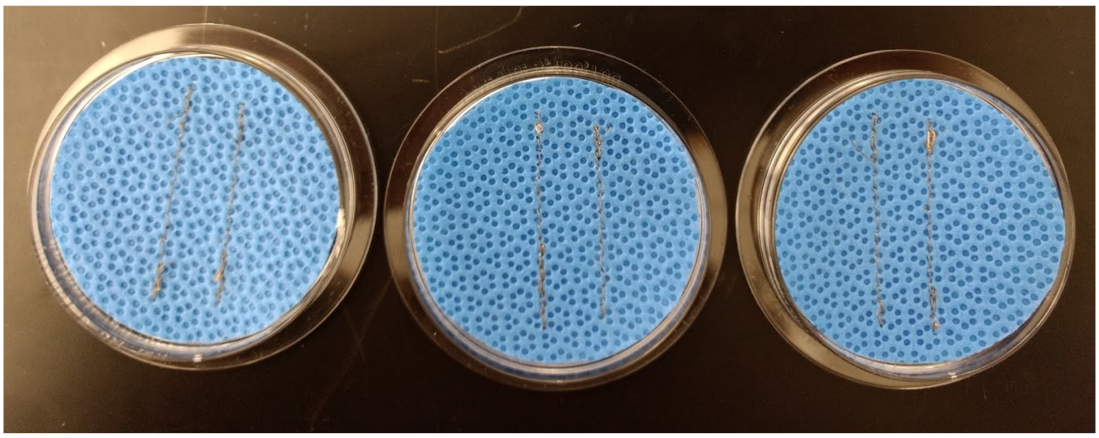

Supplemental Figure 2. 47 mm discs were cut from H600 sterilization wrap fabric sheets (Halyard Health, Alpharetta, GA) and stitched with two straight lines using a sewing machine. The total length of stitching on each of the three filters was 6.7, 6.5, and 7.0 cm.

Supplemental Table 1. Filtration efficiencies and mean pressure drop of filtration efficiencies.

	Filtration Efficiencies of Replicate Punches (%) (Standard Uncertainty)				Mean Filtration Efficiency (%)	Mean Pressure Drop (Pa)
	Punch #1	Punch #2	Punch #3	Punch #4	(95% Confidence Interval)	(95% Confidence Interval)
VFlex ™ (N95)	99.659% (99.649% - 99.669%)	99.67% (99.65% - 99.69%)	99.600% (99.590% - 99.610%)		99.64% (99.55% - 99.74%)	50 (32 - 69)
HVAC (MERV 16)	83.8% (83.3% - 84.3%)	79.7% (79.2% - 80.3%)	70.3% (69.5% - 71.1%)		78% (65% - 91%)	12 (3 - 22)
Filti™	81% (80% - 82%)	90.9% (90.7% - 91.2%)	93.2% (93.0% - 93.4%)	89.3% (89.0% - 89.6%)	89% (81% - 96%)	43 (31 - 55)
H600 (2 Layers)	87.5% (87.1% - 87.8%)	89.0% (88.7% - 89.3%)	89.7% (89.4% - 89.9%)		89% (86% - 91%)	124 (114 - 133)
H600 (1 Layer)	69.6% (68.8% - 70.4%)	70.7% (69.8% - 71.6%)	68.4% (67.6% - 69.2%)		70% (67% - 72%)	50 (34 - 66)
H600 Stitched	62% (60% - 63%)	65% (64% - 67%)	68.3% (67.4% - 69.2%)		65% (60% - 71%)	45 (35 - 54)
H500	66.9% (66.0% - 67.7%)	65.9% (64.9% - 66.9%)	68.4% (67.6% - 69.2%)		67% (65% - 69%)	40 (19 - 61)

Replicate intervals represent standard uncertainty, and mean intervals represent 95% confidence intervals.

Supplementary Discussion of Individual Discussion of Respirators

Sewn Sterilization Wrap

The sewn sterilization wrap was well tolerated by participants who noted its breathability and easily understandable speech. Nevertheless, the respirator presented a poor seal with multiple points of air leak including the nose, chin and cheeks. The respirator surface area is small compared to many currently marketed duckbill respirators and these leaks may be improved by extending the material outward across the cheeks and further below the jawline. Additionally, users noted difficulty with tightening the respirator straps due to lack of elasticity, with additionally restricted head motion when the lower strap was tightened with the head in a neutral position and the participants were instructed to look upward. Circumferential seal can be potentially improved with more elastic straps to provide additional tension to the sides of the respirator.

P100 Adaptor

Due to fabrication limitations users were not present for silicone molding and fitting and consequently the respirator was unable to be tested on a small sized user due to gross mismatch in size and circumferential lack of seal. Users noted easy breathability, but the hard-plastic design contacting the chin created discomfort while talking and acted as a lever during upward head motion reducing perceived seal. The strength of the straps was also insufficient to support the weight of the respirator with the attached filter and caused pulling away from the face during downward movements. While ideally respirators would have been molded individually to the end users this highlights a crucial challenge in widespread implementation.

Self-Moldable 3D Print

The Self-Moldable 3D Print respirator was well tolerated with easy breathability and speech comprehension. Users performed fit testing prior to individualized heat molding (described in supplementary methods) and noted that perceived air leaks were resolved with molding, however fit factor was not improved. Without fit testing this may lead to a false assurance of respirator fit and underscores the importance of proper fit testing. Additionally, users found the heat molding process to be difficult and cumbersome and a potential challenge to widespread implementation.

Multi-part 3D-Printed Mask

The multi-part 3D-printed respirator was poorly tolerated by users due to discomfort at the nose bridge and cheek bones from the hard-plastic fit as well as highly muffled and near incomprehensible speech. The multi-part design introduced several potential locations for air leak, most notably the lack of an O-ring rubber seal between the threads of the 3D respirator shell and filter housing. On forceful exhalation users noted potential air leak around the filter. Material and fabrication constraints are discussed in the supplemental methods and represent challenges with wide implementation of the potential N-95 respirator substitutes .

Commercial Elastomeric Respirator

The Commercial Elastomeric Respirator was poorly tolerated by users, both commented on discomfort at the bridge of the nose which may be attributable to greater tension on the upper strap necessary to achieve good fit. This was partially relieved by increasing inflation of the respirator, however fully inflating the respirator for user comfort compromised fit during real-

Ballard DH, *et al. BMJ Open* 2022; 11:e045557. doi: 10.1136/bmjopen-2020-045557

time testing. Additionally, users noted difficulty with talking due to tension placed on the jaw. Speech was highly muffled and difficult to understand. Furthermore, the weight of the filter caused subjective difficulty with fit during head motion and may explain the inconsistency in fit across fit test segments. Additionally, users commented on the difficulty of adjusting respirator tightness due to the high elasticity of the straps, which was necessary to counteract the high weight of the respirator. Iterations of this respirator with a single filter were found to be significantly more difficult to breathe through compared to those with a bifurcated adaptor that allowed for attachment of two separate filters.

REFERENCES

7. Mask Alternative. University of Florida College of Medicine Department of Anesthesiology Website. Available at: https://anest.ufl.edu/clinical-divisions/mask-alternative/#prototype2 Accessed on April 13, 2021.

8. 3D Printed N95 Replacement Mask. Barrow Neurological Institute Website. Available at: https://www.barrowneuro.org/get-to-know-barrow/barrow-innovation-center-2/3d-printed-n95-mask/. Accessed on April 13, 2021.

9. The Montana Mask. Make the Masks Website. Available at: https://www.makethemasks.com/. Accessed on October 2, 2020. Content no longer available at given website April 13, 2021; archived page available at request.

10. The "MalaMask" Project (N95 Alternative Filter). River City Labs Website. Available at: https://wiki.rivercitylabs.space/covid-19/3d-printed-masks. Accessed on April 13, 2021.

11. Surgical Innovation Fellowship. Boston Children's Hospital Website. Available at: http://www.childrenshospital.org/research/departments-divisions-programs/departments/surgery/surgical-innovation-fellowship. Accessed on April 13, 2021.